Take-off and landing forces in jumping frogs

Sandra Nauwelaerts[1,*] and Peter Aerts[1,2]

[1]*Department of Biology, University of Antwerp (UIA), Universiteitsplein 1, B-2610 Wilrijk, Antwerpen, Belgium and*
[2]*Department of Movement and Sports Sciences, University of Ghent, Watersportlaan 2, B-9000 Gent, Belgium*

*Author for correspondence (e-mail: sandran@mail.uri.edu)

Summary

Anurans use a saltatorial (jumping) mode of locomotion. A jumping cycle can be divided into four sub-phases: propulsion, flight, landing and recovery. We studied the landing phase during locomotion in *Rana esculenta* by measuring the ground reaction forces during propulsion and landing over a range of distances. Landing performance affects locomotor ability in jumping frogs. Landing and recovery together take up one third of the locomotor cycle. Peak landing forces are on average almost three times larger than propulsive forces. The forelimbs appear to be fully extended when they make contact with the substrate and absorb the first impact peak. The height of this peak varies depending on arm positioning and jumping distance. Since the stiffness of the arms stays constant over the full jumping range, it is possible that this is a limiting factor in the ability of the forelimbs to work as dampers. A spring-dashpot model is used to model the effect of arm angle at touch down. Damping during landing is performed by placing the forelimbs at an optimal angle to cancel frictional forces effectively.

Key words: locomotion, anura, frog, *Rana esculenta*, ground reaction force, jumping, spring-dashpot model.

Introduction

The approach to quantifying terrestrial locomotor performance in adult anurans has thus far been based on (1) variables characterising the propulsive phase, such as take-off velocity (e.g. Marsh, 1994; Marsh and John-Alder, 1994; Choi et al., 2000, 2003) and ground reaction forces (GRFs) measured using a force plate (e.g. Calow and Alexander, 1973; Wilson et al., 2000; Nauwelaerts and Aerts, 2003), or (2) direct measures of jumping distance (e.g. Wermel, 1934; Zug, 1972; Emerson, 1978; Hirano and Rome, 1984; Lutz and Rome, 1994; Marsh, 1994). Although these variables are considered appropriate as general performance parameters, conceptual concerns arise when examining locomotion in an ecological context. For instance, escaping from a predator means realizing a distance as large as possible between predator and prey, as fast as possible. This implies that factors other than jumping distance, take-off velocity or GRFs can become crucial in saltatory locomotion. One of these factors is the larger landing forces that inevitably result from increased take-off velocities and GRFs during propulsion. Valuable time could be lost during damping of the impact force and the recovery that follows. Simply jumping further by taking off faster may not represent the optimal ecological solution. The idea that recovery may be as important as take-off comes from the observation that during endurance tests frogs seem to have a preferred jumping distance that was smaller than their maximal jumping distance (S.N., unpublished data). This observation led to the hypothesis that it may not be ideal to increase the jumping distance beyond a certain limit because of its consequences on recovery.

A jumping cycle can be divided into four sub-phases: propulsion, flight, landing and recovery. To escape optimally, all phases must be of short duration with large displacements of the center of mass (COM). Anurans take off by extending their hindlimbs and using their forelimbs for landing. The forelimbs touch the ground and form a pivot, about which rotation of the body occurs. This can play a crucial role in supporting and stabilizing the frog as it lands (Peters et al., 1996). Since the forelimbs are considerably shorter than the hindlimbs and provide less deceleration distance, impact forces on the front limbs are expected to be high. The landing phase could therefore be a limiting factor in the jumping capacity of a frog for jumps where the frogs remain terrestrial. By determining the durations of the four sub-phases of a jumping cycle, we will answer the following question: (1) what fraction of the total locomotor cycle does the landing phase take up during saltatorial locomotion in frogs? By recording the GRFs we can answer: (2) are peak landing forces higher than peak propulsive forces in jumping frogs?

The forelimbs are not only used during landing (Peters et al., 1996), but also must perform a number of other functions. During feeding, they are used to manipulate and bring prey towards the mouth (Gray et al., 1997) and during wiping behavior, forelimb movements help to protect the skin by

keeping it moist. To realize these functions, the forelimbs need to be flexible. During the breeding season, male frogs use forelimbs in combat to repel rival males (Peters and Aulner, 2000). Males also grip females with their forelimbs during amplexus (Duellman, 1992). This activity demands strong isometric force production from the forelimb muscles with the forelimbs in a flexed position. If the forelimbs also play a major role during landing by damping the kinetic energy from the flight phase, the extensor muscles of the forelimbs are expected to work as dampers. By flexing the elbows, the impact forces can be reduced by increasing the braking distance. Performing various tasks that have conflicting demands might restrict the capacity of the forelimbs to perform landing effectively. By recording the landing forces of jumping frogs and the timing of forelimb action for a range of distances, we can answer an additional question: (3) does stiffness of the arms increase with jumping distance? Lastly, based on high-speed video recordings of the landing phase and predictions made by a spring-dashpot model, we can answer the final question: (4) does arm angle at touchdown influence the landing phase?

Materials and methods

Animals

Five adult male *Rana esculenta* L. were acquired from Centre d'élevage d'Animaux (Bray-et-Lû, France), ranging in size from 48–73 g (62±8 g, mean ± s.d.). Animals were kept in a light- and temperature-controlled room (8 h:16 h light:dark; T=20°C) in a large glass tank (150 cm×75 cm×75 cm) filled with wet sand and fed crickets once a week. In addition, 11 adult males, held in similar conditions, were used in the landing experiment to determine arm angles.

Experimental set-up

The animals were placed upon a small force plate [AMTI MC3A-6-100, AMTI, Watertown, MA, USA; Sensitivities vertical GRF (F_v)=1.35 µV/(V N) and horizontal GRF (F_h)=5.4 µV/(V N), natural frequency 300 Hz] with a top plate of 11.7 cm×12 cm and were induced to jump onto a second, larger force platform [AMTI OR6-6-2000; Sensitivities F_v=0.08 µV/(V N) and F_h=0.34 µV/(V N), natural frequency 1000 Hz] with a top plate of 50.8 cm×46.4 cm. Some cross-talk always exists when using strain-gauge type force plates, but the effect was minimized by including the correction terms in the calibration matrix. Slipping was prevented by covering the force platforms with water-resistant parquet sandpaper (P15U). To reduce mechanical noise, the small force plate was placed in a plastic container filled with wet sand. The two force plates were positioned 10–30 cm apart, to ensure a full jump distance range. Both force plates measured the three-dimensional GRFs during jumping. The output of the strain gauges was sent to an amplifier and A/D converted at 1 kHz (AMTI MCA strain gauge amplifier). Digital traces of the force platform and a signal from a LED (light emitting diode), used to synchronise force measurements with video recordings,

were read into a PC. Forces were subsequently smoothed using a fourth order zero phase shift Butterworth filter in a custom-made Labview program.

We examined landing behaviour by videotaping the jumps (high-speed video camera, Redlake, MASD Inc., San Diego, CA, USA) at 250 Hz and zooming in on the second force plate. Simultaneous lateral and frontal views were obtained by placing a mirror at a 45° angle next to the second force plate. The propulsive phase was also visible in the mirror view. In order to obtain the total jumping distance for each jump, a Sony 50 Hz camera was placed above the set-up, in order to provide a simultaneous view on both force plates. The set-up was lit using a Tri-lite light (Cool Light Co., Inc., Hollywood, CA, USA; 3×650 W).

Five jumps for each animal, resulting in a total of 25 jumps, were selected for further analysis. The selection of the trials was made on the basis of the jumping distance, aiming to obtain the largest possible distance range for each animal.

Timing variables

Three key timing variables were obtained from the high-speed video recordings: (1) timing of first contact of the arms with the force plate, (2) timing of body contact with the plate and (3) timing of full recovery (i.e. frog is back in launch position).

Force recordings and derived measurements

Horizontal forces F_h and vertical forces F_v were plotted for each jump and the resultant force F_r was computed. The angle of the resultant force was calculated for both the propulsion and landing phases.

Force profiles were used to determine the durations of the propulsion, flight and landing phases. Landing was defined as the phase from the first contact on the force plate to the time when the vertical GRF equalled the weight of the animal. Recovery was defined as the phase between the end of landing, based on the force profiles, and full recovery, based upon the high-speed video recordings.

Accelerations in two directions were determined from the force profiles. To obtain vertical acceleration $\mathbf{a}_v$, body weight BW was subtracted from F_v and divided by total body mass M_b. The first and second time integrals of the accelerations yielded the velocities v_h and v_v and the displacements d of the COM. Calculations for landing were done by starting with v_h and v_v at take-off, taking gravity into account (v_v–$\mathbf{g}t$, where $\mathbf{g}$ is the gravitational acceleration and t the duration of flight). Instantaneous power (P) profiles were calculated by multiplying force F by v. The time integral of the force profiles provided the impulses (I) and work (W) was obtained by integrating the power profiles. Total work for propulsion and landing was calculated by summing the absolute values of the maxima of the work profile in two directions. In addition, work done by only the forelimbs (W_f) was analysed separately.

Stiffness of the forelimbs K_f was calculated as GRF during landing ($F_{l,r}$) divided by resultant displacement of the COM (d_r) during landing.

Muscle-specific mechanical power was calculated from the GRFs and divided by the forelimb muscle mass $M_{m,f}$, determined as a fraction of M_b (4%, measured on two dead animals). Similar calculations were done for the hindlimbs for propulsion (hindlimb muscle mass $M_{m,h}$ taken as 15% of total M_b, measured on 40 dead animals as part of a different study; S.N., unpublished data).

Total jumping distance D_j was measured from the dorsal 50 Hz video recordings, by digitising the snout at the start and end of the jump using a NAC-1000 *XY* coordinator (NAC Image Technology, Inc., Tokyo, Japan) connected to a PC.

Spring-dashpot model

We used a simple model of a mass mounted on a linear spring and a velocity-dependent dashpot to test the effect of arm angle θ_f at the moment of touchdown on the course of the consequent landing phase. Data from a real sequence where the arms perform the whole deceleration action were used to parameterize the model, i.e. to obtain stiffness and damping coefficients. The simulation was ended when the mass was about 1 cm above the ground surface, which coincided with the body making contact with the force plate. The landing phase of the chosen sequence lasted 33 ms and ended with the body COM positioned approximately 1 cm above the force plate with a vertical velocity of zero. These landing conditions could be reproduced in the model with a stiffness value K of 70 N m^{-1} and damping coefficient c of 1.4 Ns m^{-1} with an arm angle of 125° at touchdown, so these stiffness and damping coefficients were used in all simulations. At touchdown, the model showed some residual v_h (about 50 cm s^{-1}), which in reality would be dissipated by frictional forces between body and the force plate surface, and by deformation of the body. The high-speed video recordings showed that when the forces become large, the body sometimes slipped forward during landing, illustrating this phenomenon. The forces in the spring-dashpot were similar to the GRFs measured in the real sequence: peak vertical force was approx. 3 N ($F_{l,v,max}$) and peak horizontal force ($F_{l,h,max}$) was approx. 2 N, and they both had decelerating actions throughout the landing phase. The model was used to test the effect of arm angle θ_f, increasing θ_f from 110 to 140° in 1° increments. Simulations were carried out for five jumping heights between 0.20 m and 0.40 m and for five horizontal velocities between 0.73 m s^{-1} and 2.19 m s^{-1} (or the initial value, determined from the real sequence; ±25% and ±50%).

High-speed video recordings

To test whether frogs optimise θ_f according to the spring-dashpot model, we recorded additional video material on the landing behaviour of frogs using a NAC-1000 high speed video camera at 500 Hz. We recorded a total of 90 landing phases from 11 frogs. These recordings were used to obtain arm angles at touchdown and 25 ms prior to touchdown. The change in position of the COM (calculated as the midpoint on a line drawn between snout tip and cloaca) during this period of time (25 ms) was used to estimate v_h and v_v at touchdown. Height h was calculated from v_v.

Statistical analysis

Peak forces F_{max} were compared among phases (propulsion-landing) and within phases using a paired *t*-test.

A correlation matrix of all selected variables with total jumping distance was built to test direct relationships. A second correlation matrix, with the peaks of all measured forces, was used to test within-phase (propulsion and landing) and between-phase relationships. In addition, a third correlation matrix was built to detect correlations between the durations of the four sub-phases of a jump.

We found two types of force profiles during landing, depending on whether the peak force was mediated by only the forelimbs or by a combination of forelimbs and trunk. We used a *t*-test to test for differences in peak forces and jumping distances between the two types of profiles.

To test whether frogs adjust their arm angle at touchdown, linear regressions were performed on arm angle *vs* height and *vs* horizontal velocity.

Results
Force profiles and timings

Typical force profiles (Fig. 1) show the components of the GRF in the three directions during propulsion and landing. The jumping cycle was divided into four phases: (1) propulsion, (2) flight, (3) landing and (4) recovery. Propulsion usually started with a slow increase in GRF $F_{p,h}$ in the horizontal direction (direction of movement) and $F_{p,v}$ in the vertical direction, often with a small time lag between $F_{p,h}$ and $F_{p,v}$, with $F_{p,h}$ preceding $F_{p,v}$. Peak forces, however, were reached simultaneously and did not differ significantly from each other (forces averaged over all jumps are $\overline{F_{p,h,max}}$= 0.94±0.05 N and $\overline{F_{p,v,max}}$=1.32±0.06 N, P=0.494). Propulsion lasted on average 0.187±0.008 s. After the flight phase ($\bar{t}$=0.180±0.010 s), during which no GRFs are recorded, the landing phase ($\bar{t}$=0.078±0.007 s) was initiated by the arms touching the force plate. Peak landing forces $\overline{F_{l,max}}$ differed significantly from propulsive forces (P<0.001) and were about three times greater than propulsive forces $\overline{F_{p,max}}$ ($\overline{F_{l,h,max}}$= 2.17±0.12 N and $\overline{F_{l,v,max}}$= 5.02±0.32 N). For landing forces, $\overline{F_{l,h,max}}$ differed significantly from $\overline{F_{l,v,max}}$ (P<0.001). The end of the landing phase was defined as the moment when horizontal forces become small and the vertical GRF (F_v) was approximately equal to weight (BW). This moment coincided with the start of the recovery phase ($\bar{t}$=0.150±0.019 s), the end of which was determined by high-speed recordings. On average, the duration of landing and recovery comprised 38±4% of the total cycle.

Based on the timing of body contact, we recognized two types of force profiles during landing (Fig. 1). In type I, $\overline{F_{l,max}}$ were reached while only the arms were in contact with the force plate. The timing of body contact in a type II profile preceded the timing of $\overline{F_{l,max}}$. Forces were on average higher
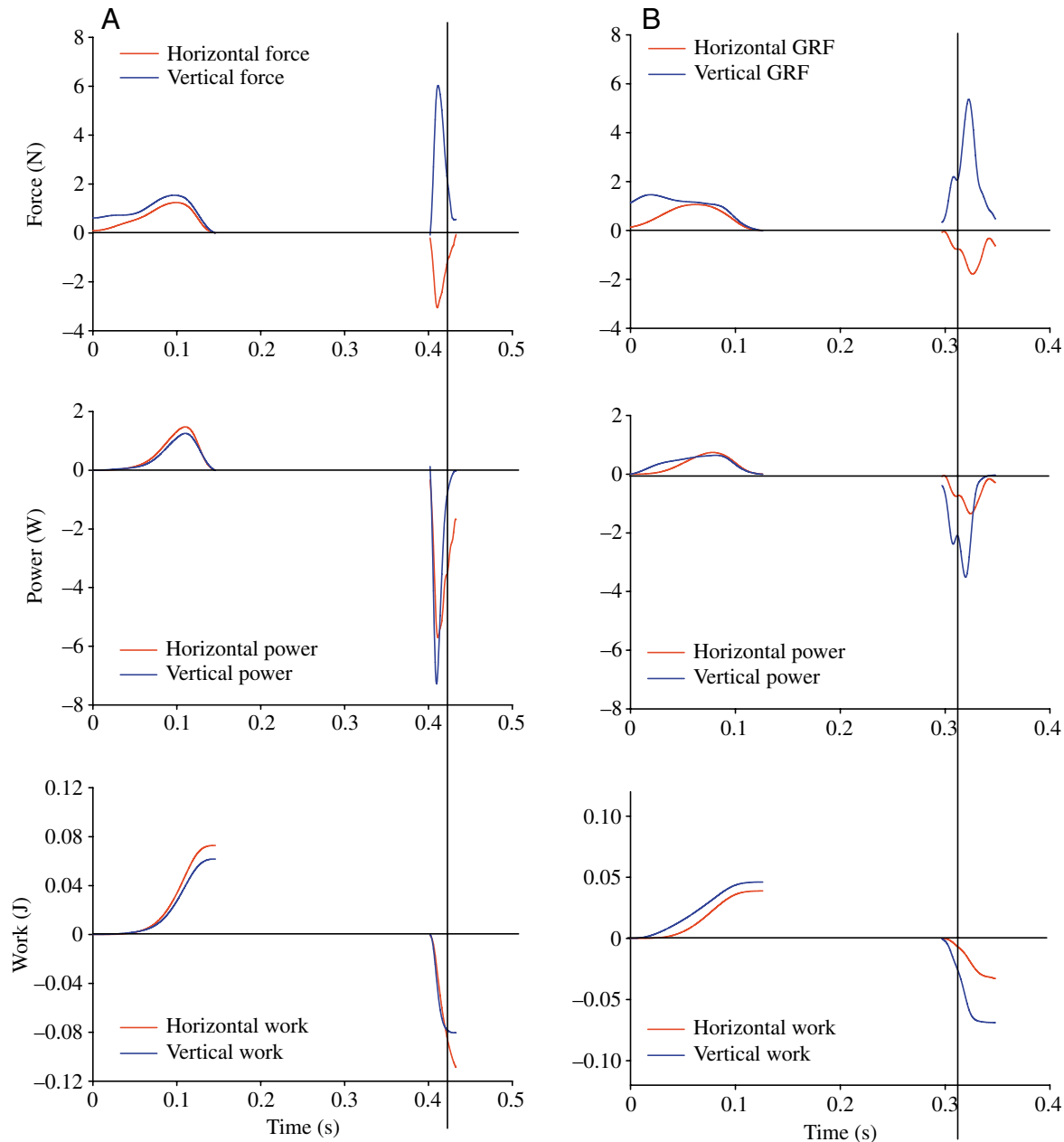
Fig. 1. Examples of force, power and work profiles of type I (A) and type II (B). Type I is defined as a profile in which the arms intercept the major force peak, while in type II profiles the timing of body contact with the force plate is prior to the timing of the peak forces. Vertical lines indicate timing of body contact with the force plate.

in type II profiles, but this did not correspond to a large difference in jumping distance (Table 1).

For the experiment in which GRFs were recorded, jumping distances D_j ranged between 0.32 m and 0.76 m. These distances were distributed equally over the five frogs and within each frog's jumping distance range. For the arm angle experiment, the animals jumped distances between 0.04 m and 0.79 m.

The angle of F_p ($\theta_{p,r}$) was fairly stereotyped (Fig. 2). At the start of propulsion phase, the resultant GRF (F_r) was directed at an angle of 88° to the horizontal (viewed from the right). $\theta_{p,r}$

decreased exponentially to around 50°, after which it increases again to an angle between 51° and 75°. At this stage, the forces became so small that the angle calculation became unreliable and usually dropped sharply to zero. In seven sequences, the angle profile decreased almost linearly from 88° to a value between 40° and 60°. However, we could not detect any differences between these seven sequences and the others, so we assumed that this slight difference in profile was due to undetermined variation. Typically, the angle profile during landing $\theta_{l,r}$ had a U shape, with a plateau around 120° and the edges increasing steeply. The timing of the angle and
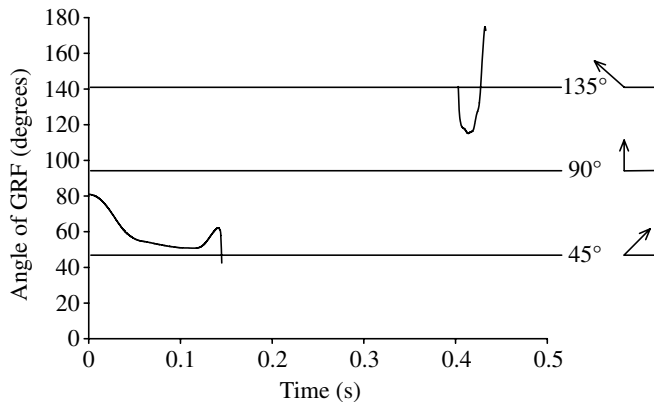
Fig. 2. An example of the angle profile of the GRF during propulsion $\theta_{p,r}$ and landing $\theta_{l,r}$.

Profile	$F_{l,h}$ (N)	$F_{l,v}$ (N)	D_j (m)
Type I	1.77±0.25	3.77±0.45	0.44±0.05
Type II	2.37±0.13	5.56±0.36	0.51±0.03
Difference	0.60	1.78	0.07
P	0.02	0.01	0.11

$F_{l,h}$, horizontal peak force during landing; $F_{l,v}$, vertical peak landing force; D_j, jumping distance.

Values are means ± s.e.m. The *t*-test analysis assumed unequal variances.

Type I, profiles in which the arms intercept the major force peak; type II profiles in which the timing of body contact with the force plate is prior to the timing of the peak forces.

magnitude of the GRF in relation to the posture of the animal is exemplified in Fig. 3 (propulsion) and Fig. 4 (landing). As previously stated, the forces during propulsion were stereotyped, while there was considerably more variation in the landing force profile.

A correlation matrix was built using the peak forces of the force components during both propulsion and landing (Table 2). Both within-phase correlations and between-phase correlations were expected between the horizontal and vertical components. Apart from the expected correlations that would occur in a purely elastic, passively behaving structure like a forward bouncing ball, $F_{p,v,max}$ also correlated significantly with $F_{l,h,max}$.

There were no significant difference in impulses of propulsion and landing, although mean impulse I during landing was mathematically smaller in both directions. ($\overline{I_{p,h}}$= 0.075±0.014 Ns *vs* $\overline{I_{l,h}}$=0.067±0.020 Ns; $\overline{I_{p,v}}$=0.154±0.034 Ns *vs* $\overline{I_{l,v}}$= 0.143±0.049 Ns).

Power and work profiles for propulsion and landing were calculated for each sequence (Fig. 1). In absolute values, peak power was on average higher during landing in both directions: $\overline{P_{p,h}}$=0.86±0.37 W   *vs* $\overline{P_{l,h}}$=−1.79±1.06 W   and $\overline{P_{p,v}}$= 0.92±0.42 W *vs* $\overline{P_{l,v}}$=−3.79±1.82 W. The values were negative for the landing phase because the energy was absorbed during this phase. Absolute total work was slightly larger during landing as opposed to the total work of propulsion, due to larger vertical work during landing. On average, $\overline{W_{p,h}}$= 0.047±0.018 J   and $\overline{W_{p,v}}$=0.056±0.021 J,   while   the corresponding values for landing were $\overline{W_{l,h}}$=−0.042±0.015 J
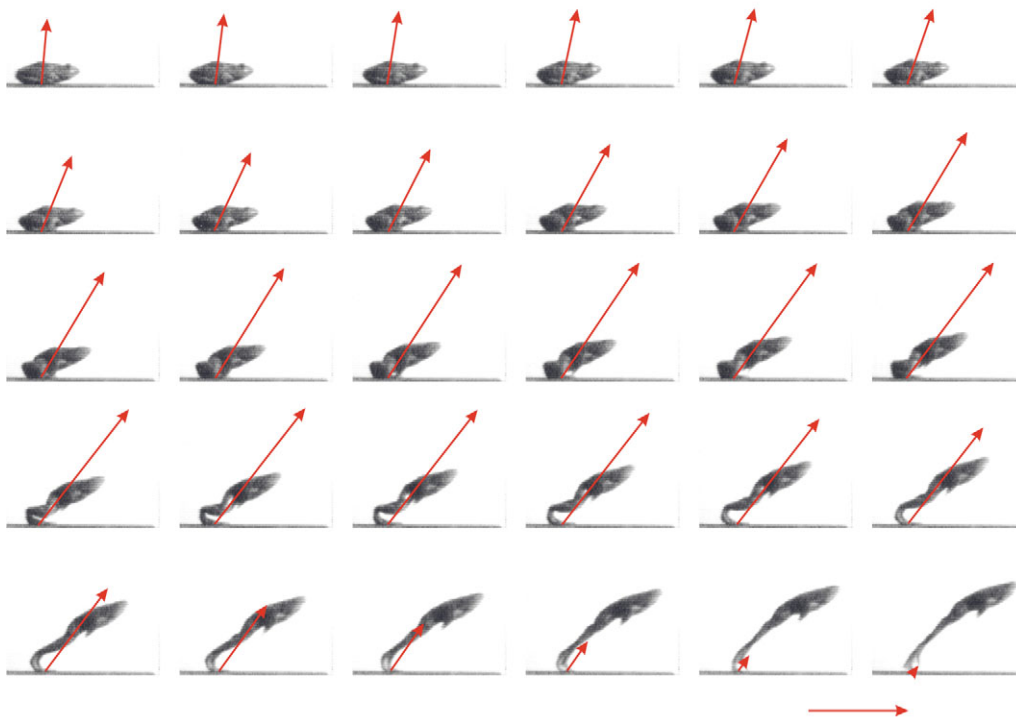

Fig. 3. Timing of body posture and angle $\theta_{p,r}$ and magnitude of $F_{p,r}$ during propulsion. Note the fact that around halfway through the propulsion phase the direction of the GRF (red arrows) runs behind the centre of gravity (which lies for a fully extended frog close to the hip). Red arrow at the bottom of the figure indicates 1N.
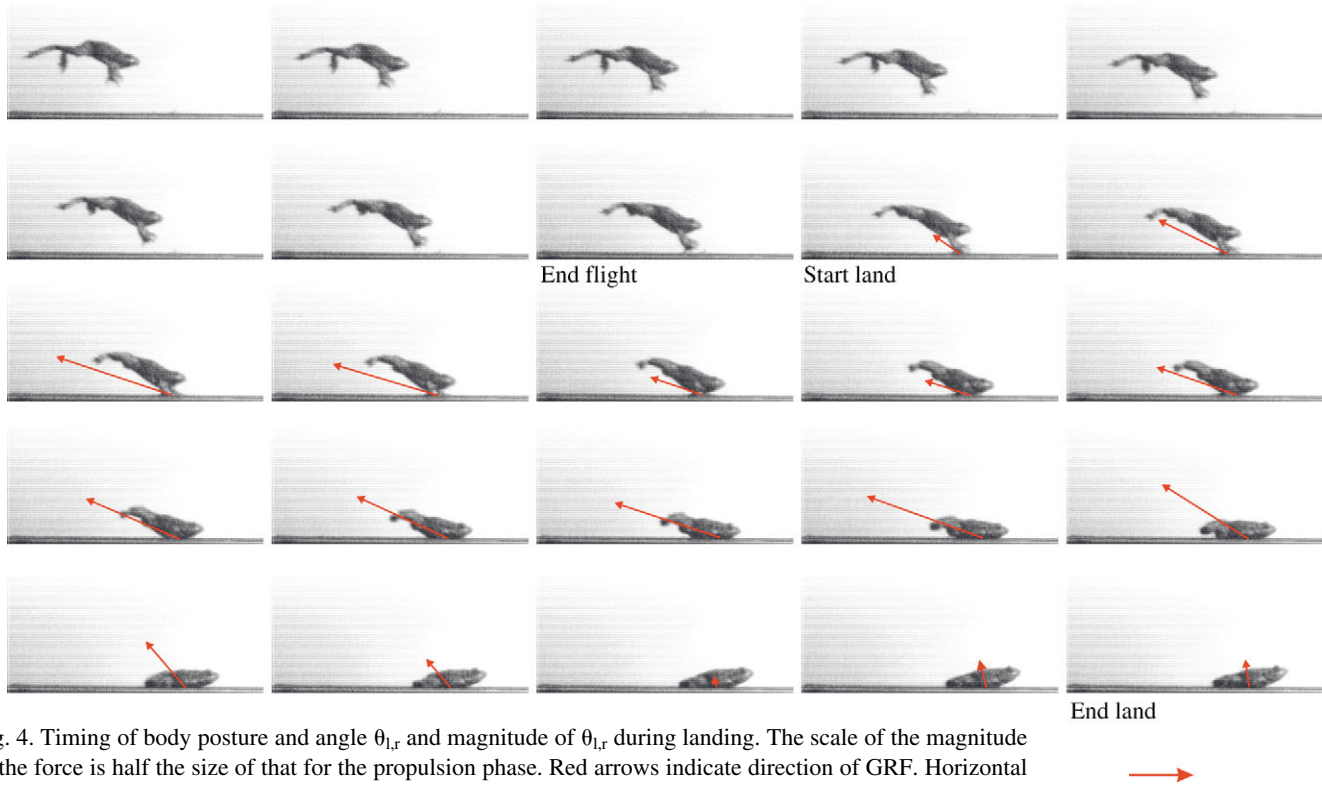
Fig. 4. Timing of body posture and angle $\theta_{l,r}$ and magnitude of $\theta_{l,r}$ during landing. The scale of the magnitude of the force is half the size of that for the propulsion phase. Red arrows indicate direction of GRF. Horizontal arrow at bottom of figure indicates 1N. Note that the scale differs between Fig. 3 and Fig. 4.

and $\overline{W_{l,v}}$=–0.067±0.032 J. The work delivered by the front limbs was on average $\overline{W_{l,h,f}}$=–0.024±0.011 J and $\overline{W_{l,v,f}}$= –0.053±0.030 J, which meant that the front limbs delivered 55±20% of the total negative work in the direction of the movement and 78±22% of the total vertical negative work. Muscle mass specific power for propulsion was on average 195±16 W kg^{-1} and maxima up to 338 W kg^{-1}; for landing the muscle mass specific power was on average –2292± 218 W kg^{-1} with maxima up to –5000 W kg^{-1}.

Mean stiffness of the hindlimbs $\overline{K_h}$ during propulsion was on average 14±1 N m^{-1}, while mean front limbs' stiffness $\overline{K_f}$ was on average 100±5 N m^{-1}.

Changes with jumping distance

To determine which variables change with distance, a correlation matrix of all variables was built (Table 3). The

Table 2. *Correlation matrix of all force components*

	$F_{p,h,max}$	$F_{p,v,max}$	$F_{l,h,max}$	$F_{l,v,max}$
$F_{p,h,max}$	0	+	+	ns
$F_{p,v,max}$		0	+	+
$F_{l,h,max}$			0	+
$F_{l,v,max}$				0

Positive correlations with jumping distance are indicated by +.

$F_{p,h,max}$, peak horizontal GRF during propulsion; $F_{p,v,max}$, peak vertical GRF during propulsion; $F_{l,h,max}$, peak horizontal GRF during landing; $F_{l,v,max}$, peak vertical GRF during landing.

$F_{p,h,max}$ increased with total jumping distance while $F_{p,v,max}$ remained constant over the range of jumping distances. In contrast, both $F_{l,h,max}$ and $F_{l,v,max}$ increased with jumping distance. More positive $W_{p,h}$ and more negative $W_{l,h,f}$ were delivered with increasing distance. Stiffness of the arms K_f was constant over the jumping distance range.

Correlations within the phase durations and with distance D_j are shown in Table 4. There was a significant positive correlation between the duration of propulsion and the duration of landing. This was due to a shared negative correlation with jumping distance. Flight duration was positively correlated with distance. Finally, the duration of recovery was only correlated with F_h of landing (not shown).

Effect of arm angle

A lateral view of the path of the model mass at landing is shown in Fig. 5 for three simulations with different arm angles. Fig. 5A, with the arms at an angle θ_f of 125° from the horizontal, is based upon a real sequence in which the data were used to tune the model (see Materials and methods). The spring-dashpot becomes shorter and rotates to a vertical position during landing. To show the considerable effect of the arm angle on the course of the landing, two scenarios are shown where only the arm angle has been changed. An increase of the arm angle to 140° yields a totally different result (Fig. 5B): the arms will rotate in the opposite direction to the 125° scenario and impact velocity on the body will be much greater, especially for the vertical velocity (1.5 m s^{-1}). Decreasing the arm angle to 110° results in a landing where

Table 3. *Correlation matrix between the force components, and their derived variables and jumping distance*

	F	**a**	v	d	P	I	I/M_b	W
Propulsion								
Horizontal	+	+	+	ns	+	ns	+	+
Vertical	ns	+	+	ns	ns	+	ns	ns
Result	+		+	ns				ns
Landing								
Horizontal	+	+	ns	ns	ns	ns	ns	ns
Vertical	+	+	ns	ns	ns	ns	ns	ns
Result	+		+	+				ns
Arm								
Horizontal	+							–
Vertical	+							ns

Positive correlations with jumping distance are indicated by +, negative correlations by –; ns, non-significant correlations. F, force; **a**, acceleration; v, velocity; d, displacement; P, power; I, impulse; M_b, body mass; W, work.

Table 4. *Correlation matrix with all phase durations and jumping distance*

|	Propulsion	Flight	Land	Recovery	Distance
Propulsion	0	ns	+	ns	–
Flight		0	ns	ns	+
Land			0	ns	–
Recovery				0	ns
Distance					0

Positive correlations with jumping distance are indicated by +, negative correlations by –.

the arms will rotate over the vertical and will flip backwards, and horizontal velocity will be high at body impact (Fig. 5C).

We also investigated the effect of changing the input parameters, height and horizontal velocity, mimicking the effect of different take-off conditions. The optimal angle at which the arms are best placed clearly depends on these conditions. The optimal angle was defined as the angle for which impact will be smallest, with impact being expressed as the velocity squared (v_r^2) at the moment the mass would hit the ground. This was done because landing means dissipating kinetic energy. The corresponding angle at the point of intersection between horizontal v_h^2 and vertical v_v^2 was chosen

as the optimal angle (Figs 6 and 7). Varying the height of the jump will principally influence the vertical velocity at impact, but horizontal velocity will also be affected to a lesser degree (Fig. 6). The optimal angle decreases linearly with increasing height. The linear equation through these data points can be used to predict the optimal angles over a wider range of

Fig. 5. Lateral view of the displacements of the COM, from touchdown (red circle) until the COM is situated 1 cm above the ground surface (body contact), resulting from the simulations of the spring-dashpot model. The time difference between two circles is 0.005 s. (A) A simulation for the real sequence, where the arm angle at touchdown is 125°, resulting in the spring-dashpot becoming shorter and rotating to a vertical position during landing. (B) The arms are put further forward, at an angle of 140°, which results in the arms stretched forward at the moment of body contact. (C) When the arm angle is decreased to 110°, the arms rotate over the vertical position during landing and the frog will land with its front limbs stretched backwards.
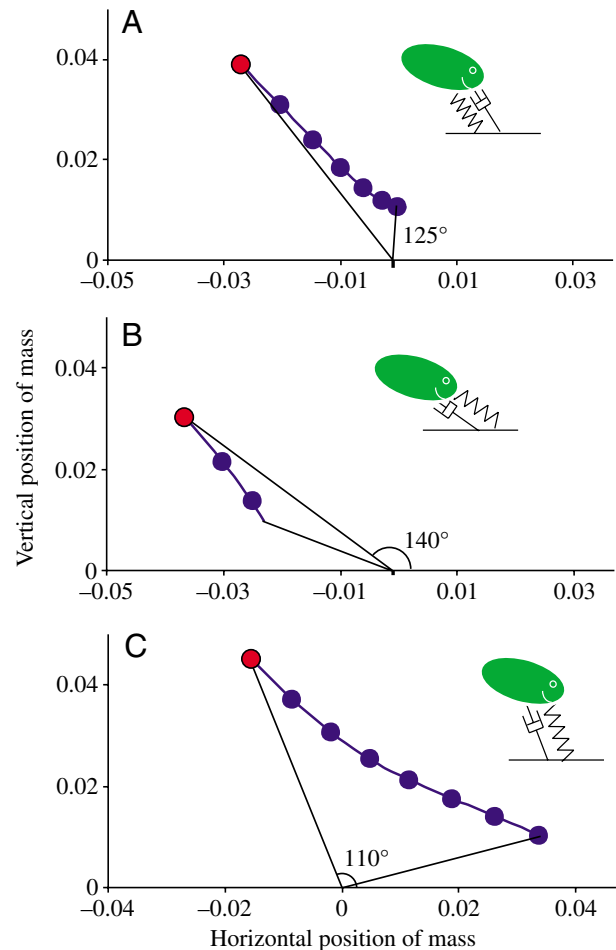
heights. We plotted the angles that were observed during additional high-speed recordings of landing and superimposed the predicted equation for optimal angle *versus* height (Fig. 6). There is considerable scatter in the measured data, but θ_f increased significantly with height (P=0.048), but not with horizontal velocity (P=0.29). The predicted value of θ_f is an overestimation when height is taken as a crucial factor (P<0.001, d.f.=89). On the other hand, when the optimal angle is calculated from its relationship to horizontal velocity (Fig. 7), the measured data do not differ from the predicted data (P=0.45, d.f.=89).

Discussion

At the start of propulsion, the GRFs increase slowly during the positioning of the trunk, first in the fore–aft direction while F_v remains at BW, and then more rapidly in both directions when the leg segments start to extend. Peak F_r is attained when hip and knee extensions are almost complete. Thus, frogs make full use of the acceleration distance (Nauwelaerts and Aerts, 2003). The GRF decreases rapidly during the roll-off of the digits (the metatarsals and the phalanges). The horizontal force pattern is similar to the force profile of a jumping galago (Günther et al., 1991). The vertical force profile, however, is different because it is more symmetrical. Both species (*Rana* and *Galago*) do not use a countermovement while jumping, making the first part of the force profile similar.

Halfway through the propulsion phase, the GRF runs behind the centre of gravity, building up an angular impulse that results in a clockwise angular momentum at take-off (looking at an animal that jumps from left to right). Due to conservation of angular momentum, the body rotates around its centre of gravity during flight. This makes the frog land on its forelimbs instead of its hindlimbs. In *Galago*, this mid-air rotation is avoided by dorsi-flexion of the tail, which counterbalances the torque of the trunk's inertia (Günther et al., 1991). The fact that there is considerable variation in landing forces probably means that the frogs are not always performing the landing phase optimally, causing the landing phase to be less predictable, although we could detect some general patterns.

What fraction of the total locomotor cycle does the landing phase take up during saltatorial locomotion in frogs?

Landing and recovery phases together comprise more than one third of the jumping cycle during which the frog is essentially not moving forward. Combined with the one third that is taken up by the flight phase, the saltatory way of
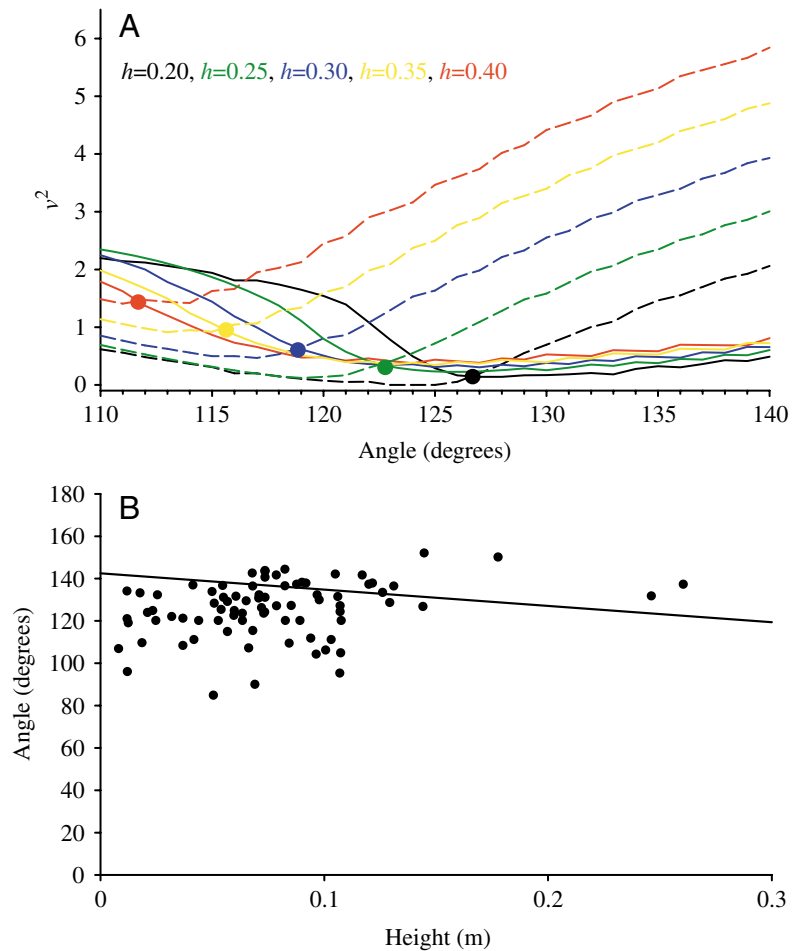

Fig. 6. (A) Vertical (solid lines) and horizontal (broken lines) velocity squared (v^2) at the moment of body contact against arm angle at touchdown. The effect of a change in height h of the jump becomes visible in the difference between the colours. Optimal arm angle is defined as the arm angle for which both v^2 are minimal (at the intersection of the solid and the broken lines) and is shown for each height as a full circle. From this graph we could determine the relationship between optimal angle and height, which we used to verify our predictions. (B) The relationship between optimal angle and height is shown as a solid line on top of a scatterplot showing the observed arm angles at touchdown against the height of the jump. Regression equation, angle= −77×height+142.5; units for v^2, $m^2 s^{-2}$.

locomotion may cause the frog's trajectory to be highly predictable and therefore easy to intercept by a predator. Taking smaller jumps can increase the maneuverability because the animal would be able to change direction during the propulsive phase and would, in theory, spend less time on the same spot during landing and recovery. However, the frogs do decrease landing duration when they jump further, suggesting that they are not working against their limits to damp the kinetic energy from flight and they are motivated to decrease all phase durations. The duration of recovery was not correlated with distance, but was correlated with $\bar{F}_{\bar{h}}$ during landing, which does suggest that a larger jump will take up more recovery time if the arms are not placed optimally (see further).
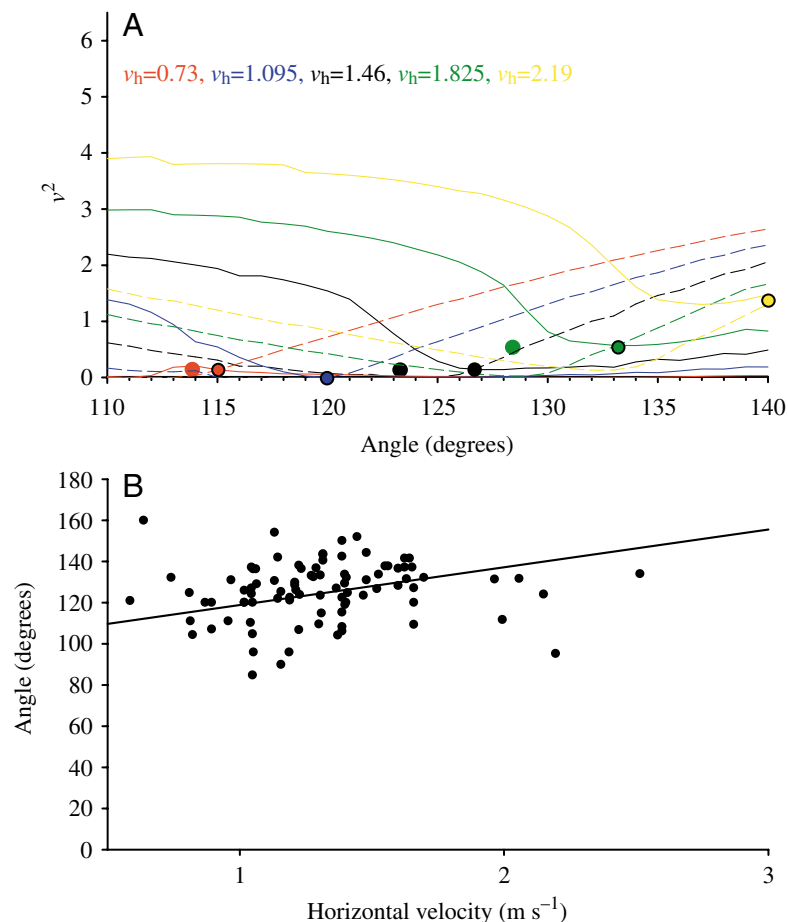
Fig. 7. (A) Vertical (solid lines) and horizontal (broken lines) velocity squared (v^2) at the moment of body contact against arm angle at touchdown. The effect of a change in horizontal velocity of the jump becomes visible in the difference between the colours. Optimal arm angle is defined as the arm angle for which both v^2 are minimal (in the crossing of the solid and the broken lines) and is shown for each horizontal flight velocity as a full circle. From this graph we could determine the relationship between optimal angle and horizontal velocity, which we used to verify our predictions. (B) The relationship between optimal angle and horizontal velocity is shown as a solid line on top of a scatterplot showing the observed arm angles at touchdown against the horizontal velocity of the jump. Regression equation, angle=18×horizontal velocity+100.5; units for v^2, m^2 s^{-2}.

Are landing forces larger than propulsive forces in jumping frogs?

Peak landing forces are on average almost three times larger than propulsive forces and landing phase duration is more than two times shorter. Both peak forces are probably overestimations of the maximal forces in the field because muddy surfaces decrease the peak forces through damping. Compliant surfaces are known to decrease the vertical force peaks through energy absorption (Demes et al., 1995; Giatsis et al., 2004). When we normalize the force data by dividing the forces by total BW, we obtain a 2.7 factor for the propulsive forces, similar to the 3.5×BW reported by Hirano and Rome (1984). The normalized landing forces amounted to 9.2×BW. Only studies on primates (Demes et al., 1995; Demes et al.,

1991) and birds (Bonser and Rayner, 1996) are available for comparison of the landing forces. Although take-off forces for birds are in a range similar to the frogs' propulsive forces, their landing forces are much smaller (1.8×BW). Birds are capable of altering their landing mechanics with their wings (Green and Cheng, 1998). Primates, on the other hand, attain much higher forces during take-off (9.6–10.3×BW), but have lower landing forces (6.7–8.4×BW: Demes et al., 1999). It has been stated that primates change their posture during flight to improve aerodynamic performance (Demes et al., 1991) and possibly their landing conditions. Many primates and birds use the same limbs for take-off and landing, making the potential acceleration and deceleration distance the same. In frogs, the forelimbs are much shorter than the hindlimbs. This means that the potential acceleration and deceleration distance is different, causing the landing forces inevitably to be larger if propulsion and landing have the similar duration.

Does stiffness of the arms increase with jumping distance?

Since the stiffness of the arms K_f stays constant over the full jumping range, it is possible that this is a limiting factor in the ability of the forelimbs to work as dampers. Human legs and other mammalian locomotor limbs also maintain a constant stiffness, regardless of speed during normal running (Glasheen and McMahon, 1995; Farley et al., 1993), but the stiffness of the leg spring doubles when humans hop in place at different frequencies (Farley et al., 1991). Because of the constant stiffness regardless of speed, the forelimbs of a frog can be regarded as locomotor limbs, unlike the human arm that operated differently by increasing its stiffness with speed (Glasheen and McMahon, 1995). Limb stiffness depends on the torsional stiffnesses of the joints and the geometry of the musculoskeletal system (Farley et al., 1998; Ferris and Farley, 1997). It is also affected by muscle activation (Morasso et al., 1999) and GRF alignment (Farley et al., 1998). In our definition of stiffness, we used the resultant GRF. This force does increase with jumping distance, so the arms compress more with distance. This is easy to achieve by bending the elbows outwards. There is, however, a limit to how much they can bend before the frog's trunk hits the ground. By controlling arm stiffness, frogs can absorb the first impact peak with their forelimbs. However, this is limited by forelimb length and, during long jumps, the highest peak will be absorbed by a combination of forelimbs and trunk. In addition to elbow flexion, the pectoral girdle is probably used as a damper. In frogs, the scapula is divided into two parts. The two scapula parts articulate through a joint that could contribute to damping during landing. In addition, the upper part (suprascapula)

is mainly cartilaginous (Shearman, 2005). Ranids have a firmisternal pectoral girdle in which the epicoracoids are fused midventrally. It has been hypothesized that a firmisternal girdle is less useful for landing than an arciferal (overlapping halves) girdle because the cartilages rotates in the horizontal during landing in the latter girdle, allowing the animal to decelerate over a greater distance (Emerson, 1988). However, the coracoid of the firmisternal girdle was not found to be loaded anywhere close to the breaking strength of the bone and seems to perform as well as an arciferal girdle (Emerson, 1983). Also, no correlation was ever found between pectoral morphology and jumping ability in frogs (Emerson, 1984). A thorough comparative functional morphological study during landing in frogs seems to be necessary to further elucidate the function of the pectoral girdle.

Maximal power generated by the hind limb muscles exceeds 300 W kg^{-1} muscle, which is near the theoretical maximum, meaning that all the muscle fibers of all hind limb muscles should be recruited and contributing directly to the mechanical power, unless some form of power amplifier is present. It has been hypothesized that these supra-maximal powers result from the rapid release of strain energy from elastic elements (Marsh, 1999; Roberts and Marsh, 2003). Such power amplifiers have been shown in other animals (Aerts, 1998; Bennet-Clark, 1975) and usually rely on a preloading of elastic components by muscular action (Roberts and Marsh, 2003), causing muscle tension to built up followed by a rapid release and a sudden increase in velocity and therefore in power. The maximal powers generated during landing are even more extreme. Since the muscles work eccentrically during braking, the muscle specific power output is expected to be 1.5–2 times higher (Rijkelijkhuizen et al., 2003; James et al., 1996) than the power output during concentric work. Our data far exceed this maximum. Rotational stiffness was not considered. The protactor muscles in the forelimbs are very small and we therefore assume that most of the damping was done passively. The high power output, together with the fact that stiffness does not increase with jumping distance, seems to confirm the presence of a passive viscous damper that can either be the pectoral girdle (see earlier) or the frog's body through deformation.

Does arm angle/position at touchdown influence the landing phase?

If the take-off and landing conditions are the same, as for a bouncing elastic ball, we would expect there to be correlations, due to ballistics, between the force components of the same direction because the angle of the GRF during take-off would be complementary to that for landing. Although these correlations are observed in jumping frogs, the unexpected, additional correlation between the *Z*-force of propulsion and the *Y*-force of landing indicates that this landing angle of the GRF is actively changed. The angular momentum and the difference in stiffness between the front- and hindlimbs are the most plausible causes of this angle change. The role of the front limbs during landing proved to be considerable. Two types of

jumps were observed, depending on whether the impact peak was mediated by the arms or by the body. Although the peak forces were on average larger when the body mediated the forces, no clear arm function limits could be detected in peak force, power or work. A mechanical limit is highly likely, but could be hard to detect because of its interaction with the positioning of the arms. The spring-dashpot model shows a spectacular effect of arm angle on the course of the landing phase (Fig. 5). In the simulation that was based on a real sequence, landing with an arm angle of 125° caused a rotation of the arm during landing to a vertical posture at body contact, purely due to the spring-dashpot action. Positioning the arms at an angle of 110° or 140° at touchdown results in a higher impact and a body posture with the arms flapped backwards and forwards respectively, thus hampering recovery. Frogs increase the arm angle with the height of the jump. When we define the optimal angle as that for which the kinetic energy at the moment of body contact is minimal in horizontal and vertical directions, the optimal arm angle is found to increase with horizontal velocity and to decrease with height. The measured arm angle of the landing frogs follow the predictions of the optimal arm angle calculated from the horizontal velocity. Avoiding remainders of horizontal kinetic energy at body contact, that would have to be cancelled by frictional forces, seems to be of major importance.

List of symbols and abbreviations

a	acceleration of the COM
a$_v$	vertical acceleration of the COM
BW	body weight
c	damping coefficient
COM	center of mass
d	displacement of the COM
d$_r$	resultant displacement of the COM
D$_j$	jumping distance
F	force
F$_f$	GRF on the forelimbs
F$_h$	horizontal GRF
F$_l$	GRF during landing
F$_{max}$	peak GRF
F$_p$	GRF during propulsion
F$_r$	resultant GRF
F$_v$	vertical GRF
$\overline{F}$	GRF averaged over all sequences [plus all combinations of subscripts: phase (p, propulsion/l, landing), direction (h, horizontal/v, vertical/r, resultant), max.]
GRF	ground reaction force
g	gravitational acceleration
h	height of the jump
I	impulse
$\overline{I_{p,h}}$	horizontal impulse during propulsion averaged over all sequences
$\overline{I_{l,h}}$	horizontal impulse during landing averaged over all sequences

$\overline{I_{p,v}}$	vertical impulse during propulsion averaged over all sequences
$\overline{I_{l,v}}$	vertical impulse during landing averaged over all sequences
K	stiffness
K_f	stiffness of forelimbs
K_h	stiffness of hindlimbs
$\overline{K_f}$	stiffness of forelimbs averaged over all sequences
$\overline{K_h}$	stiffness of hindlimbs averaged over all sequences
M_b	body mass
$M_{m,f}$	forelimb muscle mass
$M_{m,h}$	hindlimb muscle mass
P	power
$\overline{P_{p,h}}$	horizontal peak power during propulsion averaged over all sequences
$\overline{P_{l,h}}$	horizontal peak power during landing averaged over all sequences
$\overline{P_{p,v}}$	vertical peak power during propulsion averaged over all sequences
$\overline{P_{l,v}}$	vertical peak power during landing averaged over all sequences
t	duration
T	temperature
v	velocity of the COM
v_v	vertical velocity of the COM
v_h	horizontal velocity of the COM
W	work
W_f	work by the forelimbs
$W_{p,h}$	horizontal work during propulsion
$W_{l,h,f}$	horizontal work during landing by the forelimbs
$W_{p,v}$	vertical work during propulsion
$W_{l,v}$	vertical work during landing
$\overline{W_{p,h}}$	horizontal work during propulsion averaged over all sequences
$\overline{W_{l,h,f}}$	horizontal work during landing by the forelimbs averaged over all sequences
θ_f	arm angle at touchdown
θ_r	angle of F_r
$\theta_{p,r}$	angle of F_r during propulsion
$\theta_{l,r}$	angle of F_r during landing

References

Aerts, P. (1998). Vertical jumping in *Galago senegalensis*: the quest for a hidden power amplifier. *Phil. Trans. R. Soc. B* **353**, 1607-1620.

Bennet-Clark, H. C. (1975). The energetics of the jump of the locust *Schistocerca gregaria*. *J. Exp. Biol.* **63**, 53-83.

Bonser, R. and Rayner, J. (1996). Measuring leg thrust forces in the common starling. *J. Exp. Biol.* **199**, 435-439.

Calow, L. J. and Alexander, R. McN. (1973). A mechanical analysis of a hindleg of a frog (*Rana temporaria*). *J. Zool.* **171**, 293-321.

Choi, I. H., Shim, J. H., Lee, Y. S. and Ricklefs, R. E. (2000). Scaling of jumping performance in anuran amphibians. *J. Herpetol.* **34**, 222-227.

Choi, I. H., Shim, J. H. and Ricklefs, R. E. (2003). Morphometric relationships of take-off speed in anuran amphibians. *J. Exp. Zool.* **299**, A99-A102.

Demes, B., Forchap, E. and Herwig, H. (1991). They seem to glide. Are there aerodynamic effects in leaping promisian primates? *Z. Morphol. Anthropol.* **78**, 373-385.

Demes, B., Jungers, W. L., Gross, T. S. and Fleagle, J. G. (1995). Kinetics of leaping primates – influence of substrate orientation and compliance. *Am. J. Phys. Anthropol.* **96**, 419-429.

Demes, B., Fleagle, J. G. and Jungers, W. L. (1999). Takeoff and landing forces of leaping strepsirhine primates. *J. Hum. Evol.* **37**, 279-292.

Duellman, W. E. (1992). Reproductive strategies of frogs. *Sci. Am.* **267**, 80-87.

Emerson, S. B. (1978). Allometry and jumping in frogs – helping twain to meet. *Evolution* **32**, 551-564.

Emerson, S. B. (1983). Functional analysis of frog pectoral girdles – the epicoracoid cartilages. *J. Zool.* **201**, 293-308.

Emerson, S. B. (1984). Morphological variation in frog pectoral girdles – testing alternatives to a traditional adaptive explanation. *Evolution* **38**, 376-388.

Emerson, S. B. (1988). Testing for historical patterns of change: a case study with frog pectoral girdles. *Paleobiology* **14**, 174-186.

Farley, C. T., Blickhan, R., Saito, J. and Taylor, C. R. (1991). Hopping frequency in humans – a test of how springs set stride frequency in bouncing gaits. *J. Appl. Physiol.* **71**, 2127-2132.

Farley, C. T., Glasheen, J. and McMahon, T. A. (1993). Running springs – speed and animal size. *J. Exp. Biol.* **185**, 71-86.

Farley, C. T., Houdijk, H. H. P., Van Strien, C. and Louie, M. (1998). Mechanism of leg stiffness adjustment for hopping on surfaces of different stiffnesses. *J. Appl. Physiol.* **85**, 1044-1055.

Ferris, D. P. and Farley, C. T. (1997). Interaction of leg stiffness and surface stiffness during human hopping. *J. Appl. Physiol.* **82**, 15-22.

Giatsis, G., Kollias, I., Panoutsakopoulos, V. and Papaiakovou, G. (2004). Biomechanical differences in elite beach-volleyball players in vertical squat jump on rigid and sand surface. *Sports Biomech.* **3**, 145-158.

Glasheen, J. W. and McMahon, T. A. (1995). Arms are different from legs – mechanics and energetics of human hand-running. *J. Appl. Physiol.* **78**, 1280-1287.

Gray, L. A., O'Reilly, J. C. and Nishikawa, K. C. (1997). Evolution of forelimb movement patterns for prey manipulation in anurans. *J. Exp. Zool.* **277**, 417-424.

Green, P. R. and Cheng, P. (1998). Variation in kinematics and dynamics of the landing flights of pigeons on a novel perch. *J. Exp. Biol.* **201**, 3309-3316.

Günther, M. M., Ishida, H., Kumakura, H. and Nakano, Y. (1991). The jump as a fast mode of locomotion in arboreal and terrestrial biotopes. *Z. Morphol. Anthropol.* **78**, 341-372.

Hirano, M. and Rome, L. C. (1984). Jumping performance of frogs (*Rana pipiens*) as a function of muscle temperature. *J. Exp. Biol.* **108**, 429-439.

James, R. S., Young, I. S., Cox, V. M., Goldspink, D. F. and Altringham, J. D. (1996). Isometric and isotonic muscle properties as determinants of work loop power output. *Pflug. Arch. Eur. J. Phys.* **432**, 767-774.

Lutz, G. J. and Rome, L. C. (1994). Built for jumping – the design of the frog muscular system. *Science* **263**, 370-372.

Marsh, R. L. (1994). Jumping ability of anuran amphibians. *Adv. Vet. Sci. Comp. Med. B* **38**, 51-111.

Marsh, R. L. (1999). How muscles deal with real-world loads: the influence of length trajectory on muscle performance. *J. Exp. Biol.* **202**, 3377-3385.

Marsh, R. L. and John-Alder, H. B. (1994). Jumping performance of hylid frogs measured with high-speed cine film. *J. Exp. Biol.* **188**, 131-141.

Morasso, P. G. and Schieppati, M. (1999). Can muscle stiffness alone stabilize upright standing? *J. Neurophysiol.* **82**, 1622-1626.

Nauwelaerts, S. and Aerts, P. (2003). Propulsive impulse as a covarying performance measure in the comparison of the kinematics of swimming and jumping in frogs. *J. Exp. Biol.* **206**, 4341-4351.

Peters, S. E. and Aulner, D. A. (2000). Sexual dimorphism in forelimb muscles of the bullfrog, *Rana catesbeiana*: a functional analysis of isometric contractile properties. *J. Exp. Biol.* **203**, 3639-3654.

Peters, S. E., Kamel, L. T. and Bashor, D. P. (1996). Hopping and swimming in the leopard frog, *Rana pipiens*: I. Step cycles and kinematics. *J. Morph.* **230**, 1-16.

Rijkelijkhuizen, J. M., de Ruiter, C. J., Hujing, P. A. and de Haan, A.

(2003). Force/velocity curves of fast oxidative and fast glycolytic parts of rat medial gastrocnemius muscle vary for concentric but not eccentric activity. *Pflug. Arch. Eur. J. Phys.* **446**, 497-503.

Roberts, T. J. and Marsh, R. L. (2003). Probing the limits to muscle-powered accelerations: lessons from jumping bullfrogs. *J. Exp. Biol.* **206**, 2567-2580.

Shearman, R. M. (2005). Growth of the pectoral girdle of the leopard frog, *Rana pipiens* (Anura; Ranidae). *J. Morph.* **264**, 94-104.

Wermel, J. (1934). Über die Körperprportionen der Wirbeltiere und ihre funktionelle Bedeutung. Biometrische übungen Zweiter Aufsatz. Die Extremätenproportionen und der Sprung den Salientia. *Z. Anat. Entwicklungsgesch.* **103**, 645-659.

Wilson, R. S., Franklin, C. E. and James, R. S. (2000). Allometric scaling relationships of jumping performance in the striped marsh frog, *Limnodynastes peronii*. *J. Exp. Biol.* **203**, 1937-1946.

Zug, G. (1972). Anuran locomotion: structure and function. I. Preliminary observations of the relation between jumping and osteometrics of appendicular and postaxial skeleton. *Copeia* **4**, 613-624.